Calculation of stopping-power ratios using realistic clinical electron beams

G. X. Ding[a] and D. W. O. Rogers
Ionizing Radiation Standards, Institute for National Measurement Standards, National Research Council of Canada, Ottawa K1A 0R6, Canada

T. R. Mackie
University of Wisconsin, Madison, Wisconsin 53706

(Received 3 January 1994; accepted for publication 27 December 1994)

The Spencer–Attix water/air restricted mass collision stopping-power ratio is calculated in realistic electron beams in the energy range from 5–50 MeV for a variety of clinical accelerators including the Varian Clinac 2100C, the Philips SL75-20, the Siemens KD2, the AECL Therac 20, and the Scanditronix Medical Microtron 50. The realistic clinical beams are obtained from full Monte Carlo simulations of the clinical linear accelerators using the code BEAM. The stopping-power ratios calculated using clinical beams are compared with those determined according to the AAPM and the IAEA protocols which were calculated by using monoenergetic parallel beams. Using the energy–range relationship of Rogers and Bielajew [Med. Phys. **13**, 687–694 (1986)] leads to the most consistent picture in which the stopping-power ratios at d_{max} derived from mono-energetic calculations underestimate the stopping-power ratios calculated with the realistic beam by 0.3% at 5 MeV and up to 1.4% at 20 MeV. The stopping-power ratios at d_{max} determined according to the AAPM TG-21 protocol (1983) are shown to overestimate the realistic stopping-power ratios by up to 0.6% for a 5-MeV beam and underestimate them by up to 1.2% for a 20-MeV beam. Those determined according to the IAEA (1987) protocol overestimate the realistic stopping-power ratios by up to 0.3% for a 5-MeV beam and underestimate them by up to a 1.1% for a 20-MeV beam at reference depth. The causes of the differences in the stopping-power ratios between the realistic clinical mono-energetic beams are analyzed quantitatively. The changes in the stopping-power ratios at d_{max} are mainly due to the energy spread of the electron beam and the contaminant photons in the clinical beams. The effect of the angular spread of electrons is rather small except at the surface. Data are presented which give the corrected stopping-power ratios at d_{max} or reference depth starting from those determined according to protocols for any energy of clinical electron beams with scattering foils. For scanned clinical electron beams the correction to stopping-power ratios determined according to protocols is found to be less than 0.5% at d_{max} or reference depth for all beam energies studied. We quantify the differences in the stopping-power ratios determined using the depth of 50% ionization level and the depth of 50% dose level. The differences are very small except for very-high-energy beams (50 MeV) where they can be up to 0.8%.

I. INTRODUCTION

Spectrum-averaged electron restricted mass collision stopping-power ratios, denoted $(\frac{L}{\rho})^{med}_{air}$ in AAPM notation and $s_{med,air}$ in ICRU notation, play a central role in radiation dosimetry. They appear in a fundamental equation in radiation dosimetry which relates an ionization chamber reading of the charge measurement to the dose to a medium when the medium is irradiated by a photon or electron beam, viz:

$$D_{med} = M N_{gas} \left(\frac{\bar{L}}{\rho}\right)^{med}_{air} P_{ion} P_{repl} P_{wall}, \quad (1)$$

where M is the charge from the ion chamber corrected to standard atmospheric conditions, N_{gas} is the cavity gas calibration factor and the three P factors are corrections which appear in the AAPM or other dosimetry protocols.[1] The ratio of water to air stopping powers is about 15% greater for electrons with an energy of 1 MeV compared to those at 20 MeV because of the difference in density effects for the dense and gas phase media. Thus the stopping-power ratios depend strongly on the incident beam energy and increase with depth as the electrons slow down. The traditional method of determining stopping-power ratios is to assign a mean energy to the electron beam at the phantom surface, and use tabulated values of stopping-power ratios vs depth calculated for mono-energetic incident beams.

ICRU Report 35 contains a full discussion of the calculation of stopping-power ratios.[2] Several authors have reported extensive series of calculations for use in radiation dosimetry. For electron beams, Berger and Seltzer of NIST were the pioneers in the field[2,3] and their calculated stopping-power ratios for electron beams are used in the AAPM and IAEA protocols.[1,4,5]

The energy and angular distributions of electrons and contaminant photons at the phantom surface are the most important characteristics of clinical electron beams. Andreo and co-workers have shown that insufficient information about these distributions may introduce an uncertainty in dosimetry.[6,7]

If a low-energy component is added to an electron spectrum, the stopping-power ratio near the surface increases because the stopping-power ratio for low-energy electrons is higher than that for high-energy electrons. If the stopping-power ratio is calculated as if the beam were mono-energetic at the correct mean energy, then at large depths the realistic spectrum will have a lower stopping-power ratio than the mono-energetic beam because the high-energy electrons in the realistic spectrum will penetrate further and these higher-

 0094-2405/95/22(5)/489/13/$6.00

energy electrons have a lower stopping-power ratio. Based on these simple arguments, one expects the stopping-power ratio vs depth curves for a realistic beam to cross that for the corresponding mono-energetic beam. The detailed calculations of Andreo *et al.*[6,7] have confirmed this expectation.

In one paper, Andreo *et al.*[6] used the Monte Carlo method to estimate the influence of energy and angular spread on the water/air stopping-power ratios in electron beams by using simple models of the angular and energy spread of the incident electrons. For electron beams around 10 MeV they showed that beams with broad energy and angular distributions had stopping-power ratios at d_{max} which can be up to 1.0 or even 1.5% *lower* than those for mono-energetic parallel beams with the same most-probable energy. Although Andreo *et al.* derived a somewhat hard-to-use expression for relating these stopping-power ratios, they quite rightly emphasized the more important case of showing the difference between the stopping-power ratio which would be determined by using protocols to determine the mean energy at the phantom surface, $\bar{E}_0$, to establish the stopping-power ratio from the mono-energetic data, and the stopping-power ratio determined from the more realistic beam. For their simplified "realistic" beams near 10 MeV they showed *increases* of up to 0.5% might be expected at d_{max} for typical clinical accelerator beams.

Andreo and Fransson[7] extended the previous study by utilizing the actual electron and photon energy spectra and angular distributions calculated by Udale[8] for the 10-MeV beam from a Philips SL75-20 scattering-foil accelerator with a tubular applicator. They experienced difficulties since their calculated depth–dose curve did not agree either with that calculated by Udale herself with the same data nor with experiment. They convincingly showed that sampling independently from energy and angular distributions is incorrect in principle because they are highly correlated, but sampling independently was the best they, or anyone else, have been able to do. They showed that the angular distribution of the electrons, while important to their calculated depth–dose curves, had very little effect on the calculated stopping-power ratios. They also showed that the photon contamination had a "small influence" on the stopping-power ratios for this beam. Their major result was consistent with the earlier result,[6] and they estimated that the effect of the angular and energy distributions would be well less than 0.5% at d_{max}.

Klevenhagen has recently pointed out the importance of photon contamination of the incident beam when determining dose in electron beams.[9] Using several approximations and measured data for two specific accelerators, he estimated that the effect on the stopping-power ratios was to increase them by 0.3% or 0.4% at 10 MeV and up to 1.2% at 20 MeV. Aware of the lack of good data, he suggested the need for Monte Carlo calculations.

We have recently developed a very general EGS4 Monte Carlo simulation code, called BEAM, for simulating the beams from radiotherapy machines.[10] It has been extensively benchmarked against measured depth–dose curves for electron beams from seven different accelerators. By treating the energy of the mono-energetic beams from the accelerator vacuum as a parameter which was varied to match the calculated and measured values of R_{50}, it was found that depth–dose curve could be reproduced within 3% at all depths. In order to overcome the problems concerning the correlation between energy and angle,[7,8] we have stored the phase coordinates (energy, direction, position, charge) of each particle leaving the accelerator and entering the patient plane. Such realistic beams contain not only scattered lower-energy electrons but also a large number of contaminant photons, as seen in Fig. 1.

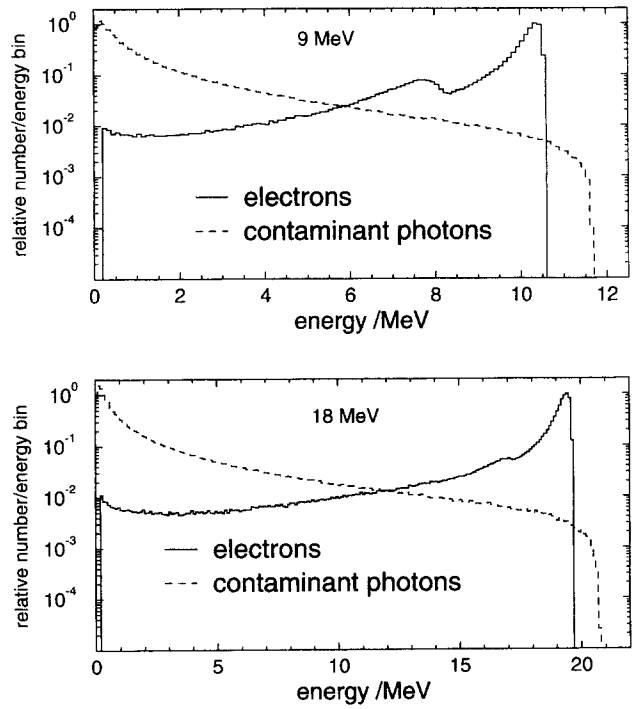

FIG. 1. The calculated spectra of electrons and photons in 9- and 18-MeV electron beams inside a 10×10-cm^2 field of a Clinac 2100C accelerator. The ratios of total contaminant photon fluence to total electron fluence inside the beam field are 1.4 and 1.7 for 9- and 18-MeV beams, respectively. Spectra calculated with BEAM (Ref. 10).

Since the beam quality varies with accelerators, particularly between scattered and scanned beam accelerators, it is important to investigate the differences in the calculated stopping-power ratios for a variety of machines. In this investigation we calculate electron stopping-power ratios in electron beams from five different clinical accelerators including the Varian Clinac 2100C, Philips SL75-20, Siemens KD2, AECL Therac 20, and Scanditronix Racetrack Microtron MM50 with an electron energy range from 5–50 MeV. Our results confirm and extend those of Andreo *et al.*[6,7] concerning the minor role of angular distributions of incident particles on stopping-power ratios. However, we will show that Andreo and Fransson[7] studied an accelerator for which photon contamination happens to play a small role. In general, although not quite as large as estimated by Klevenhagen,[9] photon contamination is important, especially at higher energies where the radiative yield increases and hence there is more photon contamination which is also higher in energy (see Fig. 1).

Following the procedure of Andreo *et al.*[6,7] our calculated results are compared with values determined according to the

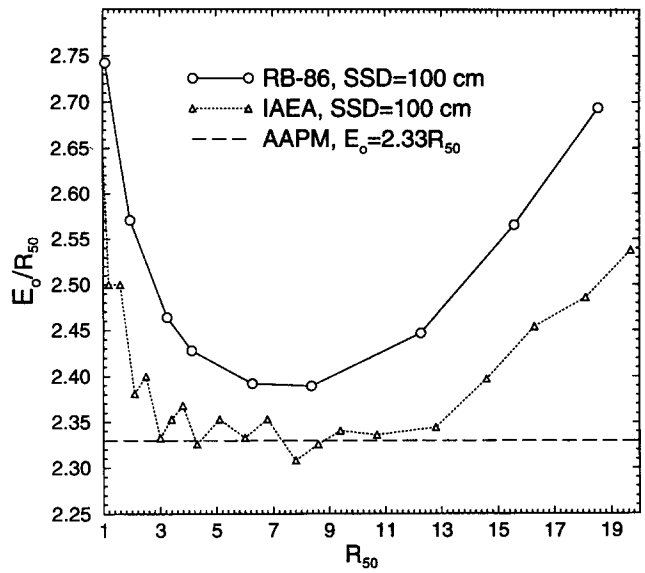

FIG. 2. A comparison of $\bar{E}_0/R_{50}$ vs R_{50} obtained from the AAPM (1983), IAEA (1987) protocol, and RB-86 (Ref. 12).

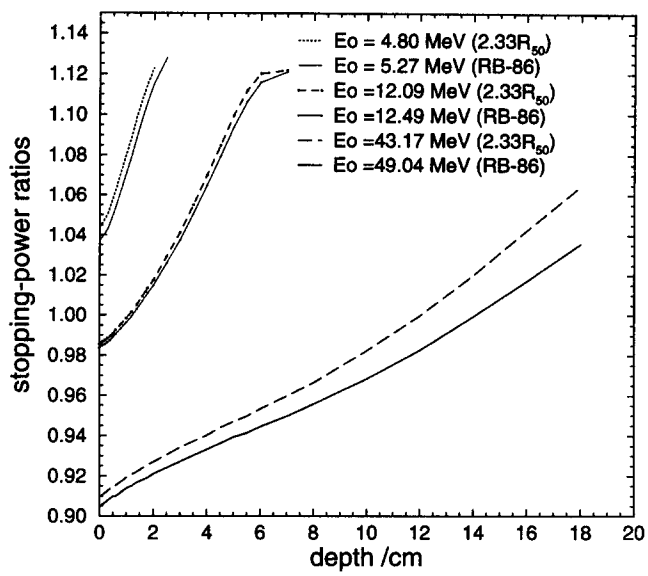

FIG. 3. The differences in mono-energetic water/air stopping-power ratios determined for energies obtained using $\bar{E}_0=2.33R_{50}$ (AAPM) or the RB-86 prescription for three R_{50} values which are typical of clinical electron beams near 5, 12, and 50 MeV. The stopping-power ratios are from the linear interpolation of values given in the AAPM protocol.

various dosimetry protocols. Correction factors have been obtained to correct the stopping-power ratios determined according the dosimetry protocols for clinical beams at d_{max} or reference depth. Protocols give water/air stopping-power ratio as a function of mean energy at the phantom surface and of the depth of measurement. The mean energy at the phantom surface, $\bar{E}_0$, is determined from the depth at which the absorbed dose or ionization falls to 50% of its maximum level. Wu *et al.*[11] pointed out that the TG-21 protocol suggested using ionization–depth curves whereas the procedure to be applied was based on data for depth–dose curves. Although the NACP and IAEA protocols take this effect into account, in Sec. IV we quantitatively examine the differences in the stopping-power ratios determined by using the 50% ionization level I_{50} instead of using R_{50}, the depth at which the absorbed dose level falls to 50% of D_{max}. In the meantime, throughout this paper, we apply the AAPM procedure to the actual absorbed-dose vs depth curves.

In the AAPM (1983) protocol[1] the mean energy of the electron beam at the surface of the phantom, $\bar{E}_0$, is given by $\bar{E}_0=2.33R_{50}$, while in the IAEA protocol[4] the relationship between $\bar{E}_0$ at the phantom surface and R_{50} at SSD=100 cm is tabulated. Using the EGS4 code, Rogers and Bielajew (RB-86)[12] calculated $\bar{E}_0/R_{50}$ as a function of R_{50} for various values of SSD. Their results are recommended for more accurate estimates of the mean energy of electron beams up to 25 MeV in the AAPM TG-25 Report.[5] The relationships between $\bar{E}_0/R_{50}$ and R_{50} obtained from the AAPM (1983),[1] IAEA (1987),[4] and RB-86[12] are shown in Fig. 2. The difference between IAEA (1987) and AAPM (1983) procedures is very small, in the energy range from 6–20 MeV. The mean energy determined according to RB-86[12] is about 400 keV higher than that determined according to the $\bar{E}_0=2.33R_{50}$ relationship for beam energies from 5–20 MeV. However, $\bar{E}_0$ determined according to the RB-86[12] and $\bar{E}_0=2.33R_{50}$ can differ by 6.4 MeV (i.e., a 13% difference) for a 50-MeV beam. The values of water/air stopping-power ratios selected using these two different mean energies can differ by up to 1% and 3% for 5- and 50-MeV electron beams, respectively, as shown in Fig. 3. Throughout this work, we have used interpolations of the tabulated data in RB-86 to determine $\bar{E}_0$ from R_{50}, not the fitted formula since it does not cover the entire energy range of interest.

II. METHOD OF CALCULATIONS

Throughout this work, stopping-power ratios determined using mono-energetic data from the AAPM TG-21 (or equivalently IAEA) protocol are determined by linear interpolation of the tabulated values in energy.

The calculation of the stopping-power ratios for realistic clinical beams in this study is carried out in two steps, viz. the generation of the clinical incident beams followed by their use as incident beams to compute the water/air stopping-power ratios.

A. The incident clinical beams

To obtain realistic clinical electron beams, a series of Monte Carlo simulations has been undertaken using the EGS4[13] user code BEAM.[10] The position, energy, charge, and direction of every particle emerging from the accelerator are stored in a "phase-space" data file. The energy cutoffs for particle transport are set to ECUT=AE=0.700 MeV (total electron energy) and PCUT=AP=0.010 MeV. In all cases, the PRESTA electron algorithm[14] is employed with ESTEPE =0.04.

The clinical electron beam field sizes are 10×10 cm^2, 25×25 cm^2, and 20×20 cm^2 for beam energies 5–20 MeV, 25–40 MeV, and 50 MeV, respectively. The SSD is 100 and 110 cm for energies 5–40 MeV and 50 MeV, respectively. In the beam simulation, the energy of electrons at the exit

vacuum window of an accelerator is adjusted to match the R_{50} between the measured and Monte Carlo calculated depth–dose curves. The depth–dose curves are calculated using the EGS4 user code DOSXYZ,[15,16] which has been extended to accept the phase-space data files as inputs.

For the accelerator beams utilized here, descriptions of the specific accelerators, relative numbers and average energies of photons and electrons and many other data, including comparisons to measured depth–dose data, are given in the BEAM paper.[10] The agreement with experiment is within 3% everywhere, and better in most cases. In particular the agreement with experiment for the 10-MeV beam from the SL75-20 accelerator is much better than obtained by Andreo and Fransson.[7] At least part of this improvement is because we could adjust the incident energy of the electron beam from vacuum to match R_{50} and include full correlation between the electron energy and angle.

B. The EGS4 user code SPRRZ

The "phase-space" data file generated by BEAM is used as input to the EGS4/PRESTA NRCC user code SPRRZ (Rogers and Bielajew, unpublished) to calculate Spencer–Attix water/air stopping-power ratios. The code SPRRZ has been used extensively[17,18] and has been shown to give the same results as previous calculations using EGS4,[19] which are, in turn, the same as previous calculations used in protocols.[1,4] The stopping powers used in the calculations are the ICRU Report 37 values[20] as implemented in EGS4.[21] The Monte Carlo code tracks the electron histories down to an energy Δ, which has been taken to be 10 keV as done in major protocols.[1,4] The code SPRRZ assumes cylindrical symmetry and the stopping-power ratios can be calculated along the central axis for columns with different radii. We find that the calculated stopping-power ratios are not sensitive to the radius as long as it is much smaller than the beam field size. For a beam with field size of 10×10 cm^2, the calculated stopping-power ratios are the same for regions with radii of 1 or 2 cm. In our calculations, a radius of 1 cm is used. The calculations are done using default PRESTA parameters[14] after tests using ESTEPE=0.01 showed that the default values were accurate.

III. RESULTS OF MONTE CARLO CALCULATIONS

A. Comparison to previous results using mono-energetic electron beams

For 9- and 18-MeV electron beams, Fig. 4 presents Spencer–Attix water to air stopping-power ratios. Two sets are calculated with the code SPRRZ and the other calculated by Berger and used in the AAPM protocol[1,3] and the IAEA code of practice.[4] Away from the surface our results calculated using plane-parallel or point source beams agree with AAPM values very well, typically within 0.1%, despite the differences in the incident beams: our point source or parallel beams have finite size (10×10 cm^2) while Berger's are broad parallel beams. Although the calculated central-axis depth–dose curves are different for the parallel and the point source beams, the energy spectra at a given depth are almost the same along the central axis. The change in the shape of the depth–dose curves is mainly caused by the change in the total electron fluence due to $1/r^2$ effects as opposed to changes in the electron spectra. Since the calculated stopping-power ratios only depend on the spectrum, the same stopping-power ratios are obtained using the parallel and point source incident beams. The higher values at the surface in the AAPM's stopping-power ratios have been discussed elsewhere[19] and reflect the assumption of charged particle equilibrium for low-energy electrons used in the calculations for the AAPM protocols.

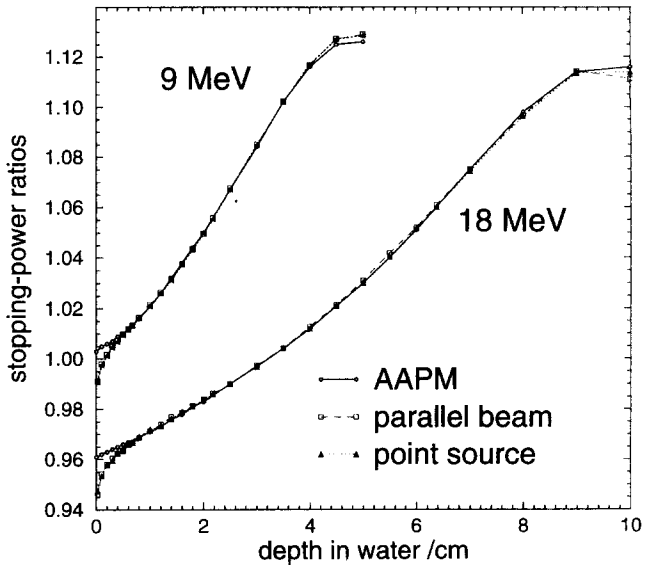

FIG. 4. For 9- and 18-MeV electron beams, comparison of the water/air stopping-power ratios calculated using code SPRRZ with a mono-energetic parallel or a point source beam and those from the AAPM protocol for broad parallel beams. The incident beams used in our calculations have finite size (10×10 cm^2). The calculated stopping-power ratios are for the beam near the central axis.

B. Results of using realistic clinical beams

Figure 5(a) shows the calculated central-axis percent depth–dose (%DD) curve for a 20-MeV electron beam from the Philips SL75-20 linear accelerator. This beam contains many scattered lower-energy electrons since the SL75-20 has fairly thick scattering foils and a solid-walled applicator. The figure also shows the dose component due to the contaminant photons incident on the water phantom. Figure 5(b) compares our calculated stopping-power ratios and those determined by using the depth, R_{50}, to establish the mean energy at the surface using $\bar{E}_0=2.33R_{50}$ or the prescription in RB-86.[12] $\bar{E}_0$ determined according to $\bar{E}_0=2.33R_{50}$ and RB-86[12] are 18.87 and 19.36 MeV, respectively. The average kinetic energy of electrons with energy above 189 keV at the phantom surface simulated using BEAM is 17.81 MeV while the most probable energy occurs at 21.2 MeV. It can be seen that stopping-power ratios determined using the RB-86[12] prescription underestimate at shallow depth and overestimate at large depth by up to 1.5% and 1.8%, respectively. In order to understand fully the causes of the deviation in the stopping-power ratios between the clinical and the mono-energetic beams we isolated each component and studied

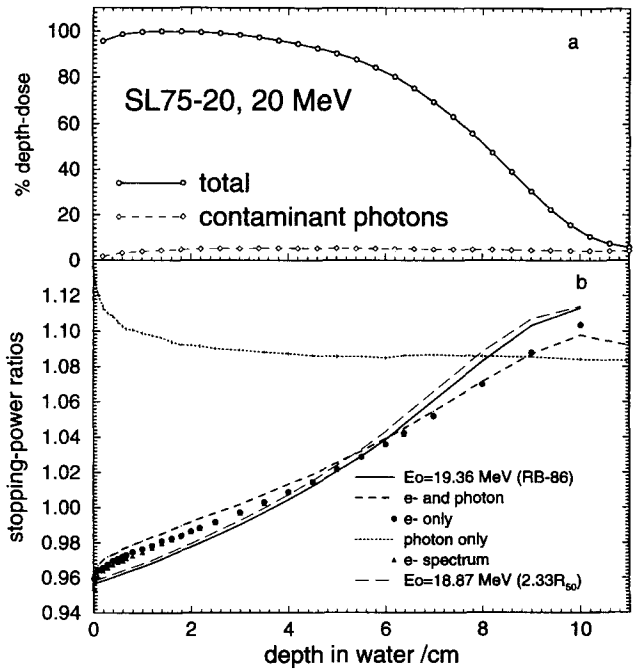

FIG. 5. (a) Calculated relative depth–dose curves for a 20-MeV electron beam from the Philips SL75-20. (b) Comparison of the water/air stopping-power ratios calculated in different ways as described in Table I.

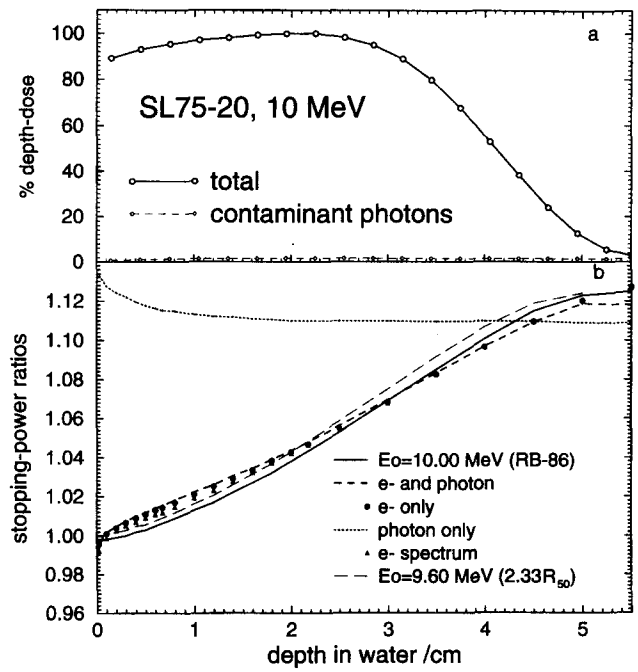

FIG. 6. (a) Calculated relative depth–dose curves for a 10-MeV electron beam from the Philips SL75-20. (b) Comparison of the water/air stopping-power ratios calculated in different ways as described in Table I.

contributions from each. Table I delineates the various types of calculations done for each beam. There is no difference in the stopping-power ratios calculated using the beam with only the electrons from the clinical beam and those calculated using a point source of electrons with the same spectrum as in the clinical beam, except for a small difference near the phantom surface. This is because the low-energy electrons in the clinical beam are often scattered from the applicator at large angles and thus affect the stopping-power ratios near the surface. The close agreement at other depths between the calculations which include all angular effects vs those coming directly from a point source at an SSD of 100 cm demonstrates that angular effects play virtually no role.

For the 20-MeV electron beam of the SL75-20 accelerator the increase in the stopping-power ratios for the clinical beam at the depth of dose maximum (≈1.5 cm) is mainly caused by the electron energy spread (≈0.9%, as shown by the difference between the curves for the mono-energetic calculations and those for the "electron only" or "electron spectrum" curves) and caused by the contaminant photons (≈0.5%, as seen by the difference between the "electron only" curve and the "electron and photon" curve for the realistic beam). Although the contaminant photons in the realistic clinical beam contribute only about 5% of the maximum dose as shown in Fig. 5(a), the influence on the stopping-power ratios is significant because the stopping-power ratios calculated from these incident photons are much higher than those from electrons (as pointed out by Klevenhagen[9]).

Similar results for a 10-MeV beam from the Philips SL75-20 linear accelerator are obtained as shown in Fig. 6. This is the same accelerator as studied by Andreo and Fransson.[7] Consistent with their results, the effects of angular distributions and photon contamination are very small for the beam. In fact, even the effect of the electron energy distribution is particularly small near d_{max} compared to values predicted using the IAEA protocol.

Figures 7 and 8 present the results for 18- and 9-MeV electron beams, respectively, from the Varian Clinac 2100C linear accelerator at the University of Wisconsin. This machine has a different beam-defining system, in particular an open applicator. The electron beam's energy spectrum is

TABLE I. Definitions of different stopping-power ratio calculations presented in Figs. 5–14.

Symbol	Caption	Type of stopping-power ratio	Energy distribution	Angular distribution
—	$\bar{E}_0$=10 MeV(RB-86)	Based on mono-energetic spr data (TG21) and $\bar{E}_0$ from RB-86	No	No
– – –	e^- and photon	Complete, realistic beam incident	Yes	Yes
●	e^- only	Electrons only from realistic beam incident	Yes	Yes
···	Photon only	Photons only from realistic beam incident	Yes	Yes
▲	e^- spectrum	Correct electron spectrum but from a point source	Yes	No
— — —	$\bar{E}_0$=10 MeV ($2.33d_{50}$)	Based on mono-energetic spr data (TG21) and $\bar{E}_0$=$2.33d_{50}$	No	No

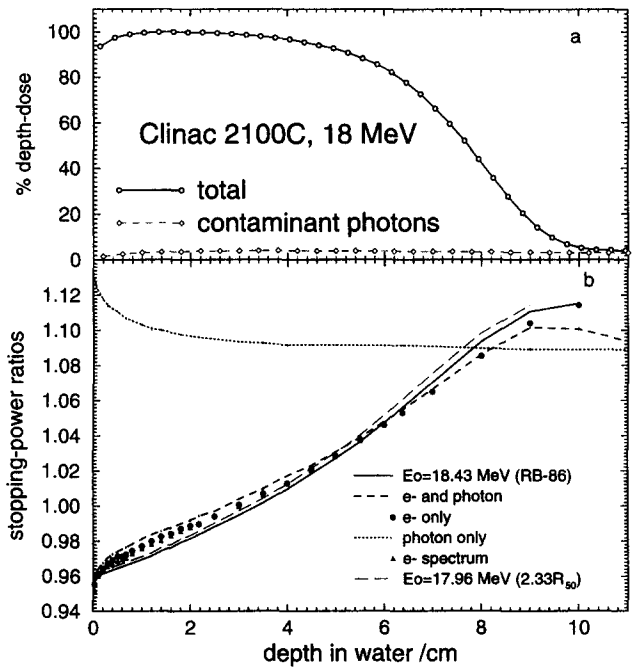

FIG. 7. (a) Calculated relative depth–dose curves for a 18-MeV electron beam from the Varian Clinac 2100C at University of Wisconsin. (b) Comparison of the water/air stopping-power ratios calculated in different ways as described in Table I.

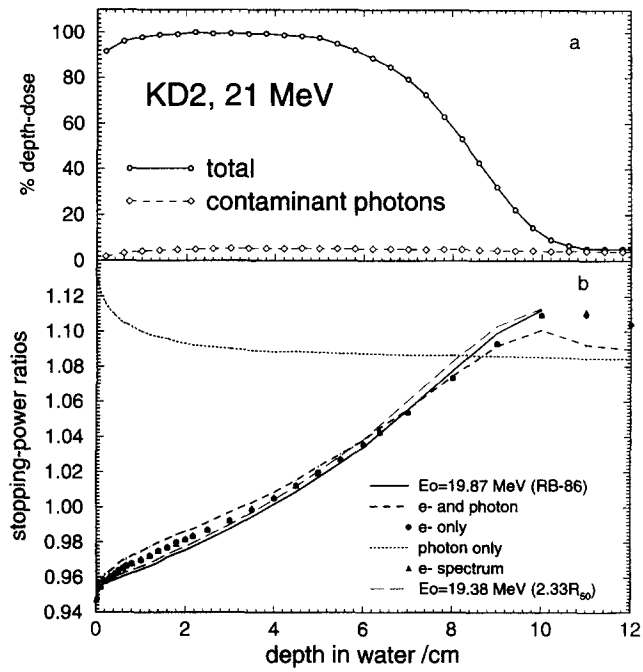

FIG. 9. (a) Calculated relative depth–dose curves for a 21-MeV electron beam from the Siemens KD2. (b) Comparison of the water/air stopping-power ratios calculated in different ways as described in Table I.

somewhat less broad and the angular spread is relatively smaller. Since the change in the stopping-power ratios due to the angular distributions is small except near the surface, similar changes in the stopping-power ratios are obtained as for the beams from the SL75-20 machine.

Figures 9 and 10 present the results for 21- and 11-MeV electron beams, respectively, from the Siemens KD2 linear accelerator. Due to its beam defining system, the beam has very little angular spread. There is no difference in the stopping-power ratios calculated using the beam with only the electrons from the clinical beam and those calculated

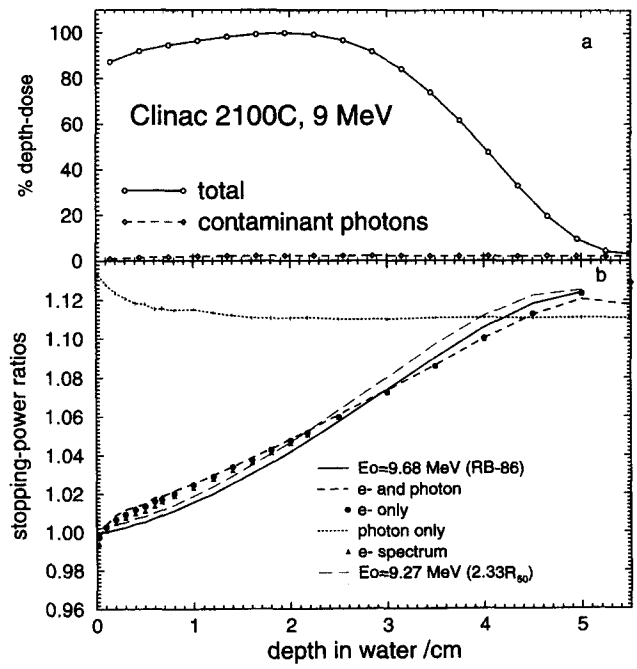

FIG. 8. (a) Calculated relative depth–dose curves for a 9-MeV electron beam from the Varian Clinac 2100C at University of Wisconsin. (b) Comparison of the water/air stopping-power ratios calculated in different ways as described in Table I.

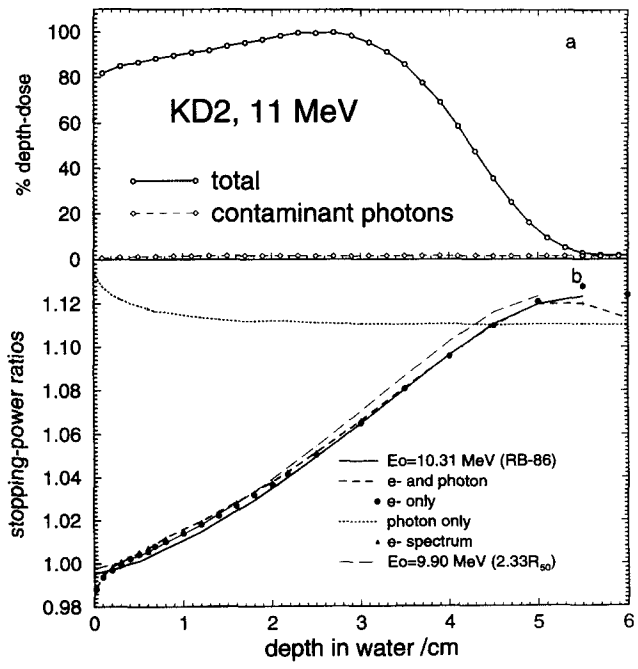

FIG. 10. (a) Calculated relative depth–dose curves for a 11-MeV electron beam from the Siemens KD2 at the General Hospital in Ottawa. (b) Comparison of the water/air stopping-power ratios calculated in different ways as described in Table I.

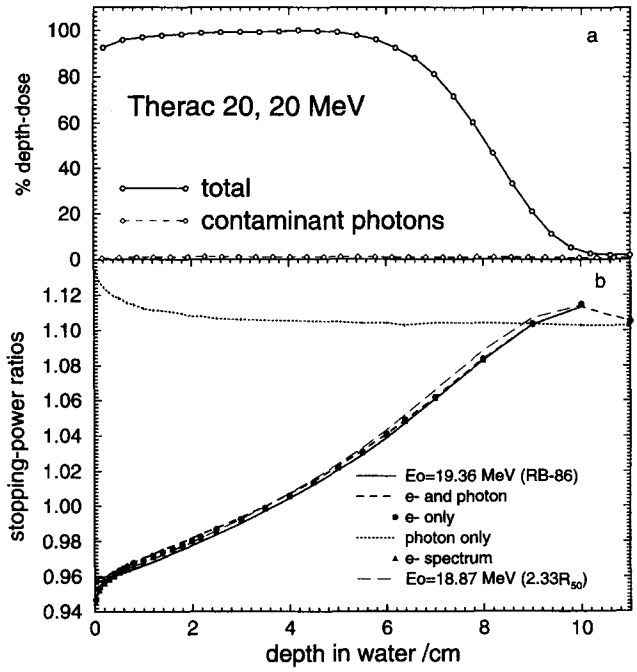

FIG. 11. (a) Calculated relative depth–dose curves for a 20-MeV electron beam from the Therac 20 at the Civic Hospital in Ottawa. (b) Comparison of the water/air stopping-power ratios calculated in different ways as described in Table I.

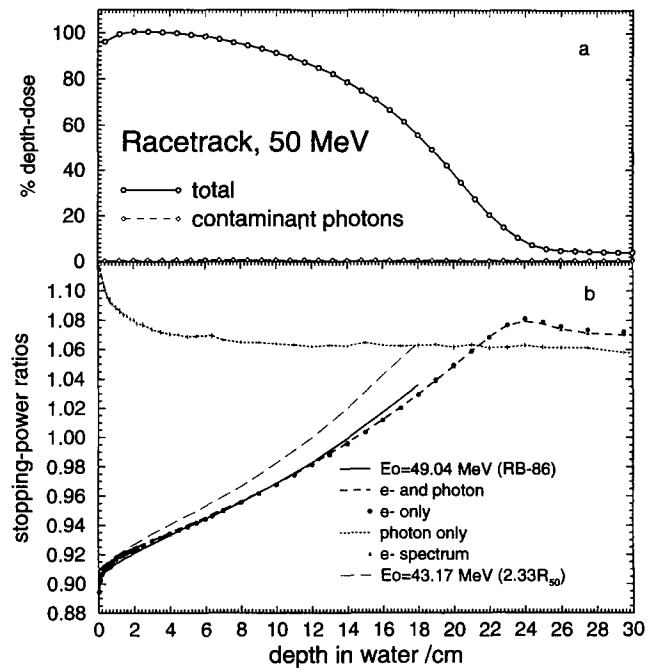

FIG. 13. (a) Calculated relative depth–dose curves for a 50-MeV electron beam from the Racetrack MM50 at Memorial Sloan–Kettering Cancer Center. (b) Comparison of the water/air stopping-power ratios calculated in different ways as described in Table I.

using a point source of electrons with the same spectrum as in the clinical beam, even near the phantom surface. The change in the stopping-power ratios due to the contaminant photons is similar to the change for the beams from the SL75-20 machine.

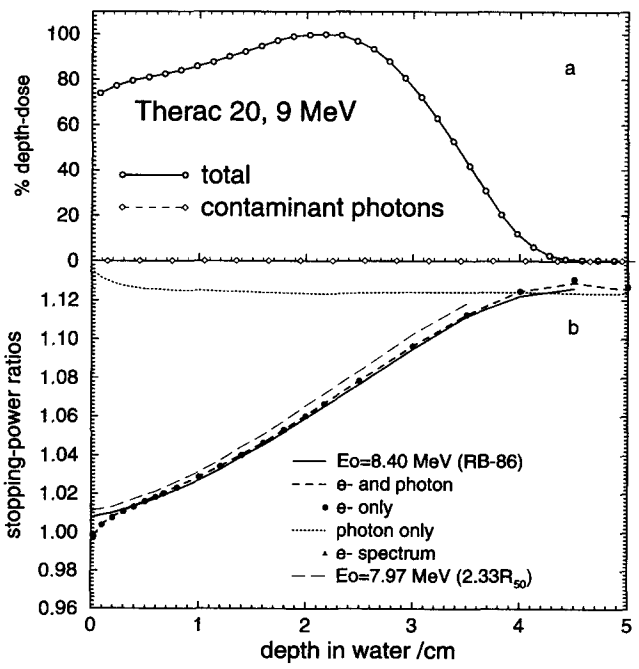

FIG. 12. (a) Calculated relative depth–dose curves for a 9-MeV electron beam from the Therac 20 at the Civic Hospital in Ottawa. (b) Comparison of the water/air stopping-power ratios calculated in different ways as described in Table I.

Figures 11 and 12 are the results from 20- and 9-MeV electron beams, respectively, from the AECL Therac 20 linear accelerator. This accelerator uses a magnetically scanned beam[10] to achieve a flat beam profile. Since there are no scattering foils, only a monitor ion chamber with a total thickness of only 0.02 g/cm^2 in the beam, there is little electron energy spread and little photon contamination. Figures 11 and 12 show that the contribution to the bremsstrahlung tail from the contaminant photons is negligible. Since the realistic beam is close to mono-energetic, there is only a small difference in the stopping-power ratios calculated using the realistic beam or by using mono-energetic stopping-power ratio data with energies determined using the RB-86[12] prescription to determine the incident mean energy.

Figures 13 and 14 give the results for 50- and 25-MeV electron beams from the Racetrack MM50 accelerator. The MM50 uses magnetic scanning to give a uniform beam. Unlike other accelerators, this machine does not have electron applicators at these beam energies. The beam field size is defined by collimators and multileaf blocks only. The beams are therefore nearly mono-energetic and have few electrons with large angle deflections. Here we see the biggest difference in selected stopping-power ratios due to the determination of $\bar{E}_0$ using RB-86[12] or the relationship $\bar{E}_0=2.33R_{50}$. It is clear that $\bar{E}_0=2.33R_{50}$ underestimates $\bar{E}_0$.

IV. DISCUSSION

A. Effects of photon contamination

The effect of contaminant photons in electron beams is to increase the stopping-power ratios in the therapeutic range as seen from the difference between the "electron only" and the

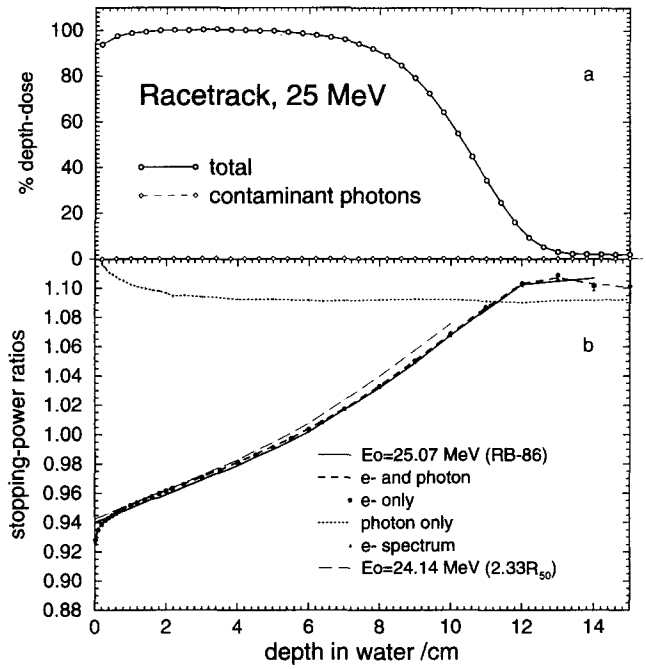

FIG. 14. (a) Calculated relative depth–dose curves for a 25-MeV electron beam from the Racetrack MM50 at Memorial Sloan–Kettering Cancer Center. (b) Comparison of the water/air stopping-power ratios calculated in different ways as described in Table I.

"electron and photon" curves in Figs. 5–14. The percentage increases due to the contaminant photons for a variety of beams (including calculations at many beam energies not shown above) are shown in Fig. 15 as a function of D_X, the percentage dose in the bremsstrahlung tail, 2 cm past the projected or practical range, R_p. As seen in the earlier figures, D_X is mostly determined by the contaminant photons except in the case of scanned beams where the bremsstrahlung tail generated within the phantom is dominant. It can be seen from Fig. 15 that the increase in the stopping-power ratios due to the contaminant photons is, not surprisingly, proportional to D_X (except for the scanned beams) and thus to the amount of photon contamination in the beam. The increases are up to 0.6% near 20 MeV. This is about half of the increase estimated by Klevenhagen[9] for similar energy beams. For beams near 10 MeV our calculations predict an 0.1% increase due to photon contamination. This is consistent with Andreo and Fransson's result[7] but less than Klevenhagen's estimate of 0.3%–0.4%.

B. Correction factors for the stopping-power ratios at reference depth

The most critical application of stopping-power ratios is for absolute dosimetry done at some reference depth, traditionally d_{max} or close to it. In this section we present the different "correction" factors to be applied to stopping-power ratios determined using the mono-energetic stopping-power ratios in the AAPM TG-21 protocol and IAEA code of practice and three different prescriptions for obtaining the appropriate mono-energetic incident beam energy, $\bar{E}_0$. The use of different prescriptions for $\bar{E}_0$ implies the corrections

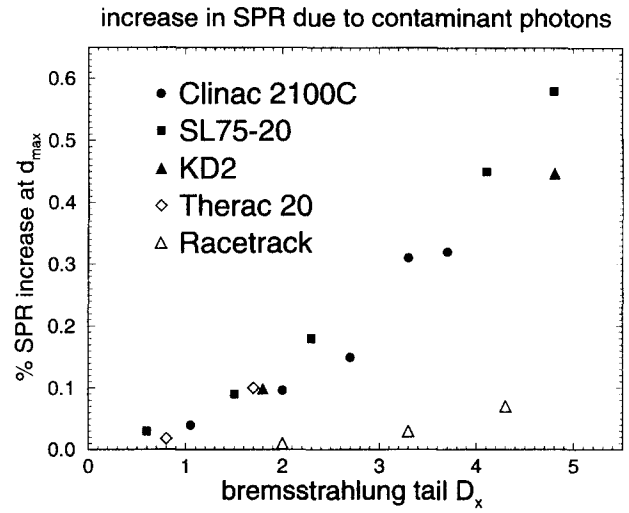

FIG. 15. The percentage increase in stopping-power ratios due to the contaminant photons in clinical electron beams versus bremsstrahlung tail D_X. The electron beam energies shown above are 6, 9, 12, 15, and 18 MeV for Clinac 2100C, 5, 10, 14, 17, and 20 MeV for Philips SL75-20, 11 and 21 MeV for Siemens KD2, 9, and 20 MeV for Therac 20 and 25, 40, and 50 MeV for Racetrack MM50.

are different, but the stopping-power ratio determined at a given reference depth in a given clinical beam is the same no matter which prescription is used, i.e., the correction factors presented also correct for any errors in the choice of $\bar{E}_0$ (and, in fact, the choice is irrelevant in this context).

Figure 16 presents the correction required for stopping-power ratios at d_{max} determined using the mono-energetic stopping-power ratio data of the AAPM TG-21 (or equivalently, the IAEA code of practice) and $\bar{E}_0$ determined following the prescription of RB-86.[12] By plotting the correction factors as a function of the bremsstrahlung tail, D_X, we find

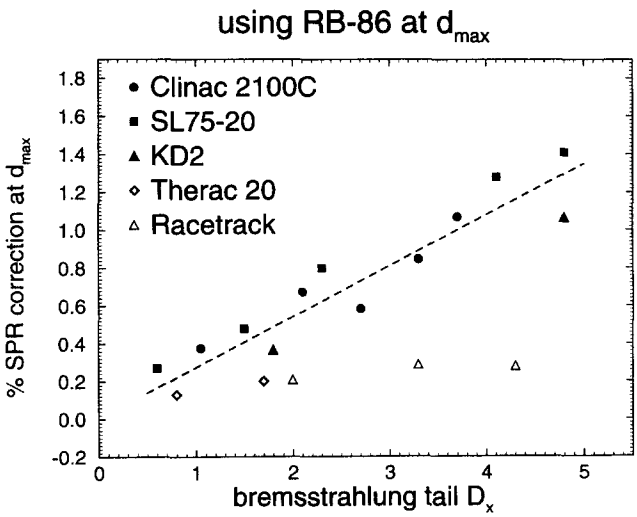

FIG. 16. The percent corrections at d_{max} to the Spencer–Attix water to air stopping-power ratios determined using the mono-energetic stopping-power ratio data in the AAPM TG21 protocol and assigning the incident mean energy using the prescription of RB-86.[12] The correction is given as a function of the bremsstrahlung tail, D_X, for the same clinical electron beams as in Fig. 15.

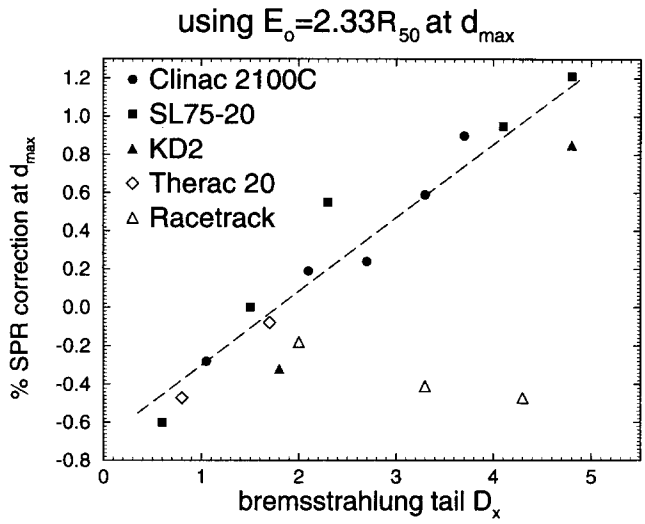

FIG. 17. As in Fig. 16, but with the incident beam energy assigned using $\bar{E}_0=2.33R_{50}$. These are the corrections needed if the TG-21 protocol of the AAPM is used.

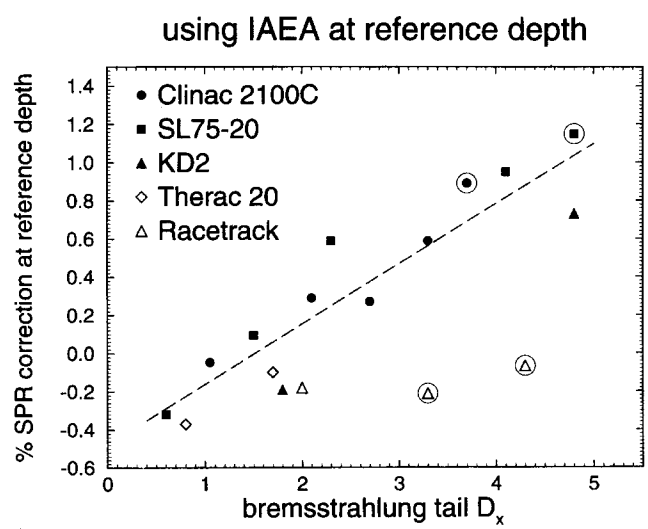

FIG. 18. As in Fig. 16, but with the incident beam energy assigned using the tabulated relationship between $\bar{E}_0$ and R_{50} found in the IAEA Code of Practice and for the stopping-power ratio at the IAEA's reference depths rather than d_{max} (see the text). Those beams for which d_{max} and d_{ref} are different are shown with a circle around the symbol.

that all values for beams with scattering foils fall close to a straight line. The scanned beam case will be discussed later.

For beams with scattering foils, the corrected water/air stopping-power ratios at d_{max} can be derived using

$$\left(\frac{\bar{L}}{\rho}\right)_{air}^{water} = (1+A_s D_X)\left[\left(\frac{\bar{L}}{\rho}\right)_{air}^{water}\right]_{RB\text{-}86}, \quad (2)$$

where the uncorrected stopping-power ratio on the right is determined using the RB-86 data for assigning the mean energy of the incident beam and the values in the TG-21 or IAEA protocols are used; $A_s=0.0027$ is a numerical constant obtained from the slope of the straight line on Fig. 16; and D_X is the percentage dose in the bremsstrahlung tail, 2 cm past R_p. For consistency, the calculated values of D_X were used to determine this equation but to apply the equation the measured values would be used. The measured and calculated values of D_X generally were found to be in excellent agreement.[10]

The bremsstrahlung tail is used to specify the corrections for the stopping-power ratios since it is convenient in clinical practice. The dose contributions from contaminant photons in the clinical beam dominate the bremsstrahlung tails in the depth–dose curve except for scanned-beam accelerators which have fewer contaminant photons. The majority of photon contamination arises in the scattering foil, which is also largely responsible for broadening the energy distribution of the primary electrons. Since the correction at d_{max} is mainly due to the electron energy spread and contaminant photons, the bremsstrahlung tail turns out (somewhat fortuitously) to be a good indicator of the correction needed.

Figure 17 presents the corrections to the stopping-power ratios at d_{max} determined as above but using $\bar{E}_0=2.33R_{50}$. As above, for beams with scattering foils, an equation can be obtained for the corrections

$$\left(\frac{\bar{L}}{\rho}\right)_{air}^{water} = (0.9932+A_{s'} D_X)\left[\left(\frac{\bar{L}}{\rho}\right)\right]_{\bar{E}_0=2.33R_{50}}, \quad (3)$$

where $A_{s'}=0.0038$ is a numerical constant obtained from the slope of the straight line on Fig. 17.

The corrections to the stopping-power ratios determined according to the IAEA protocol at reference depth are shown in Fig. 18. The reference depth is defined[4] at d_{max} for $\bar{E}_0<5$ MeV, d_{max} or 1 cm for 5 MeV$<\bar{E}_0<$10 MeV, d_{max} or 2 cm for 10 MeV$<\bar{E}_0<$20 MeV, and d_{max} or 3 cm for 20 MeV$<\bar{E}_0<$50 MeV, and the larger depth should always be chosen. Because the relationship between $\bar{E}_0$ and R_{50} given by the IAEA (shown in Fig. 2) is similar to the AAPM (1983) relationship $\bar{E}_0=2.33R_{50}$ in the energy range from 6–20 MeV, similar corrections are obtained for beams with scattering foils:

$$\left(\frac{\bar{L}}{\rho}\right)_{air}^{water} = (0.9952+A_{s''} D_X)\left[\left(\frac{\bar{L}}{\rho}\right)_{air}^{water}\right]_{IAEA}, \quad (4)$$

where $A_{s''}=0.0032$ is a numerical constant obtained from the slope of the straight line on Fig. 18.

For the three different approaches, the slope of the correction curve, or, alternatively, the maximum range of corrections, is lowest for the RB-86 method of assigning $\bar{E}_0$ and highest for the AAPM approach using $\bar{E}_0=2.33R_{50}$. This is because the RB-86 approach increases the assigned value of $\bar{E}_0$, which lowers the calculated stopping-power ratios using mono-energetic beam data. This makes the crossover point with the stopping-power ratios calculated with the realistic beams closer to the reference depth and thus leaves a smaller range of necessary corrections.

For scanned beams, corrections to the stopping-power ratios at d_{max} determined using RB-86[12] show a slight increase as the beam energy increases and corrections are less than 0.3% for all beams up to 50 MeV. The corrections to the stopping-power ratios determined according to the AAPM (1983) protocol at d_{max} or the IAEA (1987) code of practice at the reference depth show variations with energy from

-0.5% to -0.1%. The largest corrections are needed at high and low energies where the methods of assigning $\bar{E}_0$ are the most inaccurate (see Fig. 2).

For scanned beam accelerators, the beam has very little energy spread and is close to a mono-energetic electron beam with very few contaminant photons.[10] The bremsstrahlung tail is caused mainly by the bremsstrahlung photons generated inside the water phantom as seen from the depth–dose figures (Figs. 11–14). Since the RB-86 prescription for determining the mean energy of the electrons at the surface is based on EGS4 Monte Carlo calculations for mono-energetic electron beams, it is not surprising that there is very little correction required in these cases.

C. Using depth–ionization instead of depth–dose curves

In the AAPM (1983) protocol, I_{50}, the depth at which ionization falls to 50% of its maximum, is treated the same as R_{50}, the depth at which the absorbed dose falls to 50% of the dose maximum. Wu *et al.*[11] show that using the depth–ionization curve is, in principle, incorrect. A relation between I_{50} and R_{50} is given in the IAEA protocol[4,22] for broad beams at SSD=100 cm.

To study the differences in I_{50} vs R_{50}, we use our realistic beam simulations, calculated depth–dose curves, and calculated stopping-power ratios to calculate depth–ionization curves on the assumption that the ion chamber is a perfect cavity. We also assume that the measured I_{50} values include point of measurement effects (i.e., the measured ionization corresponds to that somewhat upstream of the center of a cylindrical chamber, or at the front face of a parallel plate ion chamber). For clinical beams, we find that I_{50} and R_{50} are the same only for lower-energy electron beams. A comparison between our calculated results for realistic clinical beams and values from the IAEA Code of Practice[4] is shown in Fig. 19. It can be seen that our results of $R_{50}-I_{50}$ vs I_{50} agree with the IAEA's data except when I_{50} is larger than 14 cm. The difference between I_{50} and R_{50} generally increases with the beam energy and can be estimated to within 0.4 mm by the following equation which is extracted from Fig. 19 for clinical beams with energies from 5–25 MeV ($2<I_{50}<10$ cm):

$$R_{50}=1.029I_{50}-0.063 \quad [\text{cm}], \tag{5}$$

$$I_{50}=0.972R_{50}+0.061 \quad [\text{cm}], \tag{6}$$

where R_{50} and I_{50} are in centimeters. This analysis assumes point of measurement effects have been included but ignores any change of this or other correction factors with depth, but to first order they do not affect the result.

For electron beams the increase in $\bar{E}_0$ caused by considering R_{50} instead of I_{50} is negligible at 5 MeV and up to 0.6 MeV at 22 MeV when using $\bar{E}_0=2.33R_{50}$ or using RB-86.[12] The increase can be up to 1.7 MeV for a 50-MeV beam. The range of percent errors in stopping-power ratios, δ(SPR)/SPR, introduced by using I_{50} instead of R_{50} in determining electron beam energy, is shown in Fig. 20. Only a range can be given because the difference varies with depth. The maximum difference in the stopping-power ratios is less than

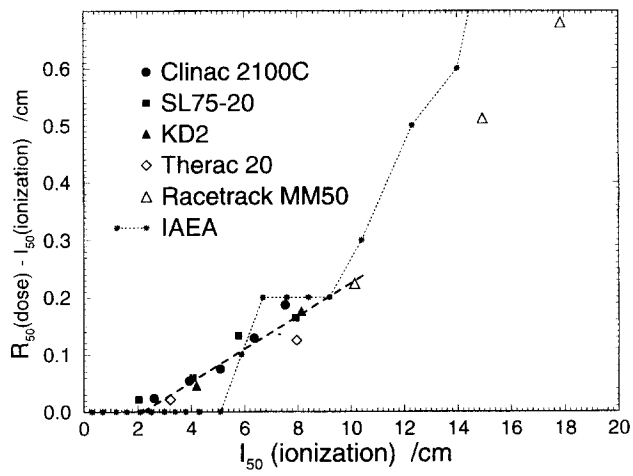

FIG. 19. The differences between the depth d_{50}, at which the depth-dose curve falls to 50% of dose maximum and the depth I_{50}, at which the depth-ionization curve falls to 50% of its maximum for clinical electron beams of energy from 5 to 50 MeV. For comparison the values provided in the IAEA Code of Practice are shown (for $I_{50}=18.2$ cm the corresponding value is 1.5).

0.8%. The minimum difference occurs at the surface while the maximum difference occurs at large depths. At d_{max} the difference is less than 0.2% for any clinical beam of energy from 5–22 MeV. If one is interested only in the central-axis depth-dose curves these differences in the stopping-power ratios have a negligible effect on the shape of the depth-dose curve although there is a significant difference between the depth-dose and depth–ionization curves.

D. Influence of electron energy spread at exit vacuum window

The electron energy at the exit window is mono-energetic in our simulations of clinical beams, but it may have some energy spread in real accelerators. Hence it is important to see whether the energy spread has an effect on our calculated

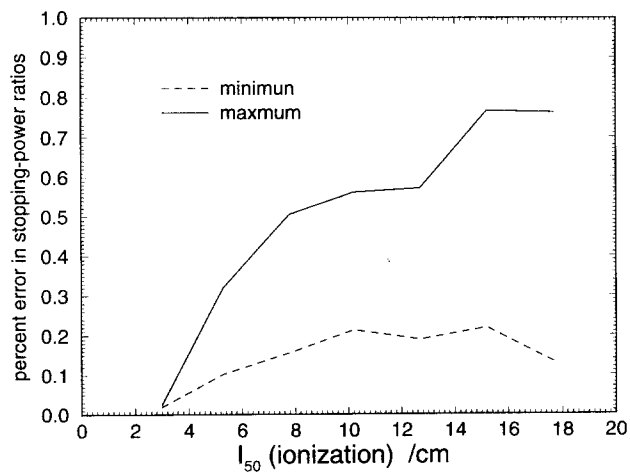

FIG. 20. The range of percent change, δ(SPR)/SPR, in the stopping-power ratios introduced by using the depth of 50% ionization level, I_{50}, instead of the depth of 50% dose level, R_{50}, for clinical electron beams of energy from 5 to 50 MeV. The percent change, δ(SPR)/SPR, is defined as $[(\text{SPR})_{I_{50}}-(\text{SPR})_{R_{50}}]/(\text{SPR})_{R_{50}}$.

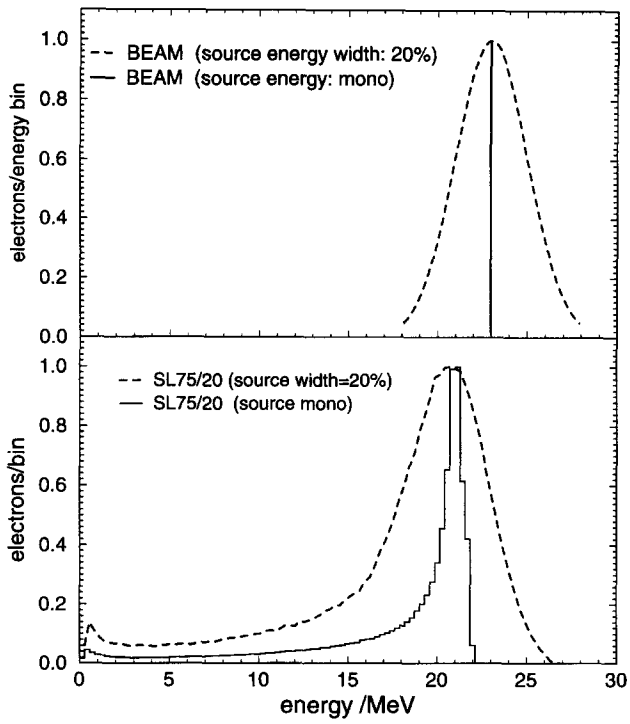

FIG. 21. (a) Electron energy spectra at the exit vacuum window. The incident energy of mono-energetic electrons is 23 MeV. The source with a 20% energy spread has a 4.7 MeV full width at half-maximum (FWHM). (b) Electron energy spectra of the SL75-20 accelerator at the phantom surface. The relative number of electrons (normalized to a peak of 1) is counted within the 10×10-cm^2 field; AE=0.521 and ECUT=0.700 MeV.

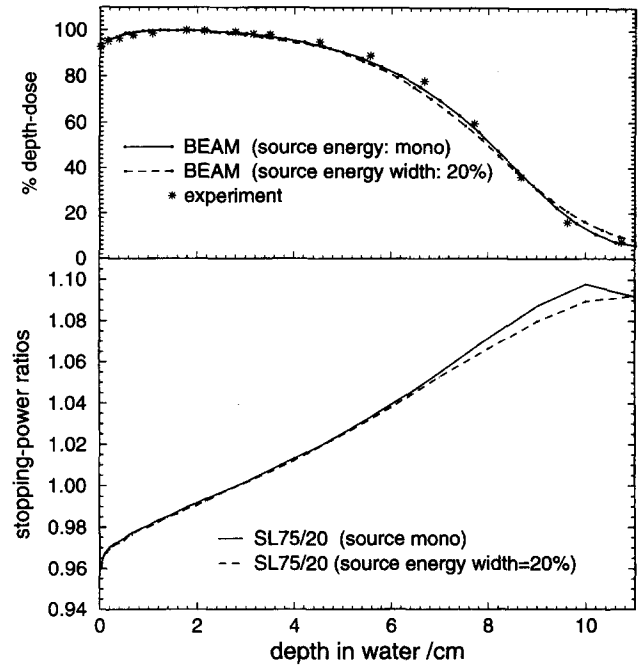

FIG. 22. (a) Comparison of the percent depth-dose curve calculated using the beam simulated with the mono-energetic source and that simulated with the source of 20% energy spread at the exit vacuum window of the accelerator SL75-20. The measured data are from Udale (Ref. 26). (b) Comparison of the water/air stopping-power ratios calculated using the two clinical beams simulated with the two energy sources at the exit vacuum windows.

stopping-power ratios. To estimate the effect we use a Gaussian function with a 4.7-MeV full width at half-maximum (FWHM) instead of a mono-energetic beam at the exit vacuum window in the simulation of a 20-MeV beam from the Philips SL75-20 accelerator. Such a large energy spread at the exit vacuum window is the worst case that can be expected in a real accelerator.[23] Figure 21 shows the electron energy spectrum at the exit vacuum window and at the phantom surface for a mono-energetic and Gaussian spread beam at the vacuum window, respectively. The energy spread at the exit vacuum window leads to a similar electron energy spread at the phantom surface. Although there is a dramatic change in the spectrum of the incident electrons, the changes in the calculated depth–dose curves and the stopping-power ratios are small, as shown in Fig. 22. There is only a small effect on the depth–dose curve because it is dominated by the electron fluence at a given depth, and this only starts to change at large depths where the low-energy electrons cannot reach. Thus we only start to observe changes there. The explanation is similar for the calculated stopping-power ratios, except in this case it is also important that stopping-power ratios vary linearly with energy and thus the average of the stopping-power ratios is the stopping-power ratio of the average energy. There is less than 0.2% change in the calculated stopping-power ratios between these two beams from the phantom surface to the depth where the dose falls to 80% of its maximum. The largest decrease ($\approx$0.8%) in the calculated stopping-power ratios occurs where the dose falls to 10% of its maximum. Figure 22 shows that the depth–dose curve calculated for the mono-energetic electron beam at the exit vacuum window is closer to the measured data than that calculated with the broad energy spectrum incident. If we use a Gaussian function with a 5% half-width (FWHM) instead of a 20% half-width (FWHM) for the energy spread at the exit vacuum window, there is negligible change in both the calculated depth–dose curve and the stopping-power ratios. These results concerning the lack of effect on the depth–dose curve are consistent with the recent results of Deasy *et al.*[24]

E. Accounting for differences in electron and photon responses of ionization chambers

As done in all previous calculations, all of our calculations ignore the difference in response of ion chambers to electrons and photons, i.e., the calculated stopping-power ratios used in Eq. (1) are based on the assumption that it is a pure electron beam. This ignores the fact that P_{wall} and P_{repl} for the photon and electron components of the beam are different.[1] Specifically, P_{wall} is usually taken as unity in electron beams but is up to 1% different from unity in photon beams and P_{repl} can be up to 6% less than unity in low-energy electron beams but is usually within 1% of unity for photon beams.

To estimate the effect of ignoring these differences on the final dose which is determined, write the overall stopping power ratio as:

$$\left[\left(\frac{\bar{L}}{\rho}\right)_{\text{air}}^{\text{med}}\right]^{\text{tot}} = (1-\gamma)\left[\left(\frac{\bar{L}}{\rho}\right)_{\text{air}}^{\text{med}}\right]^{\text{el}} + \gamma\left[\left(\frac{\bar{L}}{\rho}\right)_{\text{air}}^{\text{med}}\right]^{\text{ph}}, \tag{7}$$

where γ is the fraction of ionization in the chamber due to contaminant photons. Under these circumstances, the relative error in the dose from ignoring these differences is given by

$$\frac{\Delta D_{\text{med}}}{D_{\text{med}}} = \gamma\left(1 - \frac{P_{\text{repl}}^{\text{ph}} P_{\text{walls}}^{\text{ph}}}{P_{\text{repl}}^{\text{el}} P_{\text{wall}}^{\text{el}}}\right) \frac{\left[\left(\frac{\bar{L}}{\rho}\right)_{\text{air}}^{\text{med}}\right]^{\text{ph}}}{\left[\left(\frac{\bar{L}}{\rho}\right)_{\text{air}}^{\text{med}}\right]^{\text{tot}}}. \tag{8}$$

In the worst case and using the estimates above for P_{wall} and P_{repl}, one gets $\Delta D_{\text{med}}/D_{\text{med}} \leq 0.05 \times 0.007 \times 1.2 = 0.4\%$. However, in realistic situations, if $P_{\text{repl}}^{\text{el}}$ is far from unity (i.e., lower-energy case) so that the middle term in Eq. (8) is large, then there is little photon contamination, $\gamma \leq 0.01$, and the overall error is small. Conversely, whenever there is significant photon contamination (high-energy case) so that the γ term is large, then $P_{\text{repl}}^{\text{el}}$ is near unity and thus the middle term makes the overall expression small. Thus the error introduced is usually 0.1% or less.

V. CONCLUSIONS

We have presented detailed data on stopping-power ratios vs depth calculated using realistic clinical beams from a variety of clinical accelerators including the Varian Clinac 2100C, the Philips SL75-20, the AECL Therac 20, the Siemens KD2, and the Scanditronix Medical Microtron 50. Our results are compared with the stopping-power ratios determined using various approximations to determine the incident energy of the "equivalent" mono-energetic beam. The most self-consistent approach is to use the tabulated data from RB-86[12] since it is based on Monte Carlo calculations using the same code. This procedure takes beam divergence effects into account to obtain a more accurate mean energy than the relation $\bar{E}_0 = 2.33 R_{50}$ used in the AAPM TG-21 protocol. The IAEA Code of Practice[4] gives the energy–range relationship in a table; however, the values are close to 2.33 in the energy range from 6–20 MeV. The differences in the stopping-power ratios between our results using the realistic clinical beams and those using equivalent mono-energetic beams vary with the beam quality. Generally speaking, clinical electron beams can be classified into two types on the basis of overall beam quality: scanned beams and beams with scattering foils.

The scanned-beam accelerators, which use a magnetic field to sweep electrons to achieve a uniform distribution at the surface, produce much cleaner beams. Therefore the correction to the stopping-power ratios is rather small, less than 0.3% at $d_{\max}$ using the RB-86 procedure to assign $\bar{E}_0$ or less than 0.5% at $d_{\max}$ or at the reference depth using either the AAPM TG-21 or IAEA procedures to assign $\bar{E}_0$.

For clinical beams from those accelerators which use scattering foils to achieve a flat profile at the surface, if one uses the RB-86 prescription to assign $\bar{E}_0$, the stopping-power ratios are underestimated by up to 1.5% in regions near $d_{\max}$ and overestimated by up to 1.8% at large depths, depending on the beam energy. Our calculated results are in reasonable agreement with the calculations by Andreo *et al.*[6,7] for less sophisticated models of beams near 10 MeV, although in their particular case they were dealing with a beam in which the photon contamination plays little role and the effects of electron energy spread are negligible at the reference depth. A detailed analysis shows that the changes in the stopping-power ratios between the realistic clinical beam and those determined using calculations for mono-energetic beams and various methods for assigning the "equivalent" value of $\bar{E}_0$ are mainly caused by the electron energy spread and contaminant photons. The increase in the stopping-power ratios due to the contaminated photons in the electron beams is about 0.1% for scanned beams of all energies and is up to 0.6% at 20 MeV for beams with scattering foils. These values are not as large as those estimated by Klevenhagen,[9] but they confirm his major conclusion that these effects should be taken into account. As indicated at 10 MeV by Andreo *et al.*'s results, for all the beams studied here it has been shown that the contribution to the changes in the stopping-power ratios due to the electron angular distributions is small except at the surface.

We find that even a very substantial Gaussian spread (in fact any symmetric distribution with the same mean energy) in the energy spectrum of the electrons leaving the accelerator vacuum has very little effect on the calculated depth–dose or stopping-power ratio vs depth curves, despite directly affecting the energy spectrum of the beam on the patient plane. It is the asymmetric low-energy side of the main peak in the realistic electron beam's spectrum which has the most significant effect on the depth–dose and stopping-power ratio vs depth curves.

To make this study useful in clinical practice for reference dosimetry, we developed simple equations [Eqs. (2)–(4)] that can be used to correct the stopping-power ratios (at $d_{\max}$ or the IAEA reference depth) which were determined using any of three procedures for assigning the mean energy at the surface, $\bar{E}_0$. The equations apply to accelerators with scattering foils and are all parameterized in terms of D_x, the percentage dose in the bremsstrahlung tail. The corrections needed for scanned beams are smaller than for scatter-foil beams, especially if the RB-86 procedure is used to assign $\bar{E}_0$.

It is known that the mean energies determined according to RB-86[12] and $\bar{E}_0 = 2.33 R_{50}$ differ by about 0.4 MeV for electron beams of energy from 5–20 MeV. The difference increases for higher energy beams and it can be up to 6.4 MeV (13%) for a 50-MeV beam. The energy difference causes 1% and 3% changes in selected stopping-power ratios for electron beams of energy 5 and 50 MeV, respectively. We suggest that the mean energy should be determined using the procedure of RB-86[12] since it is inherently more accurate. A related study on the relationship between $\bar{E}_0$ and R_{50} using realistic beams confirms this.[25] However, it must be emphasized that, using the corrections presented here, the final stopping-power ratio determined is independent of which prescription for $\bar{E}_0$ is used in the clinic.

We have studied the difference between using the depth of 50% dose level, R_{50}, and the depth of 50% ionization level, I_{50}, for specifying the incident energy of clinical electron beams. The difference, $R_{50} - I_{50}$, increases with the beam

energy and can be estimated by a linear equation. Correcting the depth I_{50} to R_{50} has very small effect on $\bar{E}_0$ for low-energy beams but increases the beam energy $\bar{E}_0$ by up to 3% for a 50-MeV clinical beam. The maximum change in selected stopping-power ratios introduced by using the depth of I_{50} instead of the depth R_{50} is negligible for 5-MeV beams and up to 0.8% for 50-MeV beams. However, at d_{max} for clinical beams between 5 and 22 MeV the difference is less than 0.2%.

ACKNOWLEDGMENTS

We wish to thank Dr. Joanna Cygler of the Civic Hospital in Ottawa for providing the information needed to simulate the Therac 20, Dr. Chen Chui of Memorial Sloan–Kettering Cancer Center in New York for providing the information needed to simulate the Racetrack Microtron treatment head, Dr. Jack Janssen and Dr. Henk Huizenga of the Dr. Daniel den Hoed Cancer Clinic for information related to the Siemens KD2, and Dr. Alex Bielajew for supporting the EGS4 system at NRC. We wish to thank our colleagues Dr. Carl Ross and Dr. Charlie Ma, and the anonymous referees for their valuable comments on the manuscript. The first author (G.X.D.) is the recipient of the MRC Studentship Award and is grateful to the Medical Research Council of Canada for providing the support to do research in medical physics. This research was partially supported by NCI Grant No. ROI CA52692.

[a]Additional address: Department of Physics, Carleton University, Ottawa, Canada (613) 993-2715; E-mail: gding@irs.phy.nrc.ca; FAX: (613) 952-9865.

[1]AAPM TG-21, "A protocol for the determination of absorbed dose from high-energy photon and electron beams," Med. Phys. **10**, 741–771 (1983).

[2]ICRU, "Radiation Dosimetry: Electron beams with energies between 1 and 50 MeV," ICRU Report 35, Bethesda, MD (1984).

[3]M. J. Berger, S. M. Seltzer, S. R. Domen, and P. J. Lamperti, "Stopping-power ratios for electron dosimetry with ionization chambers," in Biomedical Dosimetry (IAEA, Vienna, 1975), pp. 589-609.

[4]IAEA, International Atomic Energy Agency, "Absorbed Dose Determination in Photon and Electron Beams; An International Code of Practice," Technical Report Series No. 277 (IAEA, Vienna, 1987).

[5]F. M. Khan, K. P. Doppke, K. R. Hogstrom, G. J. Kutcher, R. Nath, S. C. Prasad, J. C. Purdy, M. Rozenfeld, and B. L. Werner, "Clinical electron-beam dosimetry: Report of AAPM Radiation Therapy Committee Task Group 25," Med. Phys. **18** , 73–109 (1991).

[6]P. Andreo, A. Brahme, A. E. Nahum, and O. Mattsson, "Influence of energy and angular spread on stopping-power ratios for electron beams," Phys. Med. Biol. **34**, 751–768 (1989).

[7]P. Andreo and A. Fransson, "Stopping-power ratios and their uncertainties for clinical electron beam dosimetry," Phys. Med. Biol. **34**, 1847–1861 (1989).

[8]M. Udale, "A Monte Carlo investigation of surface doses for broad electron beams," Phys. Med. Biol. **33**, 939–954 (1988).

[9]S. C. Klevenhagen, "An algorithm to include the bremsstrahlung contamination in the determination of the absorbed dose in electron beams," Phys. Med. Biol. **39**, 1103–1112 (1994).

[10]D. W. O. Rogers, B. A. Faddegon, G. X. Ding, C.-M. Ma, J. Wei, and T. R. Mackie, "BEAM: A Monte Carlo code to simulate radiotherapy treatment units," Med. Phys. **22**, 503–524 (1995).

[11]A. Wu, A. M. Kalend, R. D. Zwicker, and E. S. Sternick, "Comments on the method of energy determination for electron beam in the TG-21 protocol," Med. Phys. **11**, 871–872 (1984).

[12]D. W. O. Rogers and A. F. Bielajew, "Differences in electron depth dose curves calculated with EGS and ETRAN and improved energy-range relationships," Med. Phys. **13**, 687–694 (1986).

[13]W. R. Nelson, H. Hirayama, and D. W. O. Rogers, "The EGS4 Code System," Stanford Linear Accelerator Center Report SLAC-265 (Stanford, CA) (1985).

[14]A. F. Bielajew and D. W. O. Rogers, "PRESTA: The Parameter Reduced Electron-Step Transport Algorithm for Electron Monte Carlo Transport," Nucl. Instrum. Meth. B **18**, 165–181 (1987).

[15]D. W. O. Rogers and A. F. Bielajew, "Monte Carlo techniques of electron and photon transport for radiation dosimetry," in *The Dosimetry of Ionizing Radiation, Vol. III*, edited by K. R. Kase, B. E. Bjarngard, and F. H. Attix (Academic, New York, 1990), pp. 427–539.

[16]A. F. Bielajew and D. W. O. Rogers, "A standard timing benchmark for EGS4 Monte Carlo calculations," Med. Phys. **19**, 303–304 (1992).

[17]A. Kosunen and D. W. O. Rogers, "DDSPR: A Code for calculating photon beam depth–dose curves and stopping-power ratios for an arbitrary spectrum," National Research Council Canada Report PIRS-298 (1992).

[18]A. Kosunen and D. W. O. Rogers, "Beam quality specification for photon beam dosimetry," Med. Phys. **20**, 1181–1188 (1993).

[19]C. Malamut, D. W. O. Rogers, and A. F. Bielajew, "Calculation of water/air stopping-power ratios using EGS4 with explicit treatment of electron–positron differences," Med. Phys. **18**, 1222–1228 (1991).

[20]ICRU, "Stopping Powers for Electrons and Positrons," Report 37, Bethesda, MD (1984).

[21]S. Duane, A. F. Bielajew, and D. W. O. Rogers, "Use of ICRU-37/NBS Collision Stopping Powers in the EGS4 System," NRCC Report PIRS-0177, Ottawa (March 1989).

[22]NACP, "Procedures in external beam radiotherapy dosimetry with photon and electron beams with maximum energies between 1 and 50 MeV," Acta Radiol. Oncol. **19**, 55–79 (1980).

[23]J. O. Deasy, "Electron energy and angular distributions in radiotherapy," Ph.D. thesis, University of Kentucky (1992).

[24]J. O. Deasy, P. R. Almond, and M. T. McEllistrem, "The spectra dependence of electron central-axis depth–dose curves," Med. Phys. **21**, 1369–1376 (1994).

[25]G. X. Ding, D. W. O. Rogers, and T. R. Mackie, "Mean energy, energy-range relationships and depth-scaling factors for clinical electron beams," submitted to Med. Phys. (1995).

[26]M. Udale-Smith, "A Monte Carlo Investigation of High Energy Electron Beams Used in Radiotherapy," Ph.D. thesis, Leeds University (1990).